

Article

Research on the Law of Surge Pressure during Tripping of HTHP Wells under the Influence of Tool Joints

Jiangang Shi ^{1,2}, Buwen Yu ¹ , Xianzhi Song ^{1,*} and Yong Guo ²

¹ State Key Laboratory of Petroleum Resources and Prospecting, China University of Petroleum, Beijing 102249, China

² Research Institute of Engineering Technology, PetroChina Xinjiang Oilfield Company, Karamay 834000, China

* Correspondence: songxz@cup.edu.cn

Abstract: Accurate surge pressure prediction during tripping is significant to ensure drilling safety. Based on the theory of wellbore hydraulics and heat transfer, a surge pressure prediction model considering the influence of HTHP and joints is established in this paper. The finite difference method is used to solve the wellbore flow model. Compared with the measured surge pressure, it was found that the error between the predicted and measured values after considering the above factors was only 0.89%. The influence of dimensionless joint outer diameter, joint length and drill string tripping speed on the surge pressure was further analyzed. The results show that the existence of joints increases the surge pressure. When the dimensionless joint outer diameter was increased from 0.70 to 0.91, the surge pressure increased by 76%. Neglecting the effect of the joint will cause a large error in calculating the surge pressure. In addition, the surge pressure is positively correlated with the drill string tripping speed. However, with the decrease in drill string tripping speed, the surge pressure will gradually tend to a stable value. This study provides a theoretical reference for the hydraulic design of HTHP well tripping.

Keywords: surge pressure; steady-state model; HTHP; tool joint



Citation: Shi, J.; Yu, B.; Song, X.; Guo, Y. Research on the Law of Surge Pressure during Tripping of HTHP Wells under the Influence of Tool Joints. *Energies* **2022**, *15*, 8943. <https://doi.org/10.3390/en15238943>

Academic Editor: Hossein Hamidi

Received: 2 October 2022

Accepted: 23 November 2022

Published: 26 November 2022

Publisher's Note: MDPI stays neutral with regard to jurisdictional claims in published maps and institutional affiliations.



Copyright: © 2022 by the authors. Licensee MDPI, Basel, Switzerland. This article is an open access article distributed under the terms and conditions of the Creative Commons Attribution (CC BY) license (<https://creativecommons.org/licenses/by/4.0/>).

1. Introduction

During the tripping operation, additional pressure is generated in the well. This phenomenon is called pressure surge. If the pressure increases the wellbore pressure, it is called surge pressure; otherwise, it is called swab pressure [1]. If the tripping speed is too high, the swab/surge pressure will be too large, which may destroy the wellbore pressure balance and cause complex accidents such as lost circulation and blowout. If the tripping speed is too low, although it will not cause downhole accidents, it will increase the non-productive time [2,3]. Due to the complex formation pressure in deep wells and the prominent features of HTHP, swab/surge pressure is more likely to damage the wellbore pressure balance [4,5]. Therefore, accurate swab/surge pressure prediction is crucial for ensuring the safety of deep well tripping and improving operation efficiency.

Research on pressure surge can be traced back to the 1930s, and Cannon [6] noted that “even though the drilling fluid density is much higher than the formation pressure, blowouts still occur”. To investigate this question, he conducted field experiments and measured the surge pressure due to drill string movement. Goins et al. [7] found that the movement of the drill string can also cause lost circulation, and they measured the swab pressure due to the movement of the drill string.

Since the 1950s, scholars have conducted a lot of research on swab/surge pressure. Cardwell [8] published charts for estimating swab and surge pressure. Due to the lack of understanding of drilling fluid rheology at the time, the charts were made based on Newtonian models. As a result, the practical value of these charts is not high. In 1961, Burkhardt [9] analyzed the variation law of pressure surge using field measured data,

and established a swab/surge pressure calculation model suitable for concentric annulus for Bingham fluid. The calculated results of swab/surge pressure are in good agreement with the measured data. After that, Schuh [10] established a power-law fluid swab/surge pressure calculation model using a method similar to Burkhardt. Then, Fontenot and Clark [11] improved the calculation method of pressure surge based on the research of Burkhardt and Schuh, which could realize the change of drilling fluid properties with well depth.

In 1977, Lubinski [12] established a dynamic swab/surge pressure calculation model based on the unstable flow in the well, considering factors such as drilling fluid compressibility and inertia. Based on Lubinski's research, Lal [13] evaluated the friction force as a distribution function, which improved Lubinski's research. Mitchell [14] further considered factors such as pipe elasticity and drilling fluid rheological properties and established a dynamic swab/surge pressure calculation model. In 1995, Zhong et al. [15] found a differential governing equation for fluid flow in an eccentric annulus and the calculation model of the steady-state surge pressure of the eccentric annular power-law fluid was deduced. Jeong et al. [16] conducted a tool joint pressure drop experiment and found that a tool joint would significantly affect the annular pressure. In 2012, Srivastav et al. [17] experimentally studied the effect of eccentricity and other factors on surge pressure. The results show that the drill string's tripping speed, the mud's properties, the annulus clearance, and the drill string's eccentricity greatly influence the surge pressure. In 2013, Li et al. [18] analyzed the impact of drill collars on surge pressure. The results show that if the influence of the drill collar is ignored, the surge pressure will cause a large calculation error. It may lead to complex accidents in the well. Li et al. [19] deduced the calculation model of swab/surge pressure under steady laminar flow conditions based on the R-S rheological model. They solved the model by using the adaptive Simpson integration method.

Regarding the calculation model of swab/surge pressure, previous researchers have studied the steady-state swab/surge pressure model and the dynamic swab/surge pressure model based on the assumptions of steady flow and unstable flow in the well. By considering factors such as the drilling fluid rheological mode, drilling fluid compressibility, drill string eccentricity, HTHP, etc., the swab/surge pressure calculation model was enriched and improved. The influence of parameters such as drilling fluid properties and drill string tripping speed on swab/surge pressure was analyzed. Moreover, previous studies have shown that joints significantly impact the calculation of swab/surge pressure [16,20].

However, little research on pressure surge considering the influence of joints has been seen, and no calculation model for swab/surge pressure considering both the effect of temperature and pressure on fluid properties and the existence of joints has been found. It should be noted that the causes of surge and swab pressure are similar, and the two research methods are almost identical. The main difference between surge and swab pressure is that they have opposite effects on wellbore pressure. Therefore, this paper mainly studies surge pressure. Based on the fundamental laws of fluid mechanics, this paper deduces the calculation equation of the surge pressure at the joint. Combined with the wellbore flow and heat transfer model and the prediction model of HTHP fluid properties, a calculation model of surge pressure for the HTHP well is established. Based on this model, the influence of joints and tripping speed on surge pressure is analyzed.

2. The Construction of Surge Pressure Calculation Model

2.1. Surge Pressure Caused by Tool Joints

2.1.1. The Sudden Contraction Pipe

Figure 1 is a schematic diagram of the annular drilling fluid flow in the joint section during tripping. The flow section suddenly shrinks when the drilling fluid flows from section 1-1 to section 2-2. Before the drilling fluid enters the small annulus, the main flow begins to shrink, forming a shrinking area in the small annulus and a vortex is generated between the main flow and the wall of the drill string. The drilling fluid velocity increases, and the pressure decreases at the constricted section. After that, the stream lines gradually

return to parallel straight lines. During this process, pressure changes occur due to the collision between the fluids and the generation of vortices.

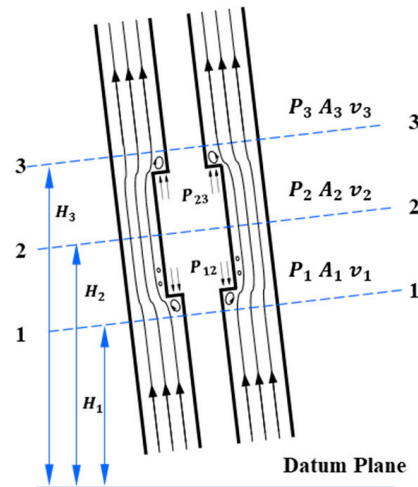


Figure 1. Schematic diagram of drilling fluid flow at the tool joint.

During the process of drilling fluid flowing from section 1-1 to section 2-2, it can be obtained from the conservation of drilling fluid mass.

$$\rho A_1 v_1 = \rho A_2 v_2 \tag{1}$$

where ρ is the annular drilling fluid density (kg/m^3), A_1 is the annular cross-sectional area of section 1-1 (m^2), v_1 is the annular drilling fluid velocity of section 1-1 (m/s), A_2 is the annular cross-sectional area of section 2-2 (m^2), v_2 is the annular drilling fluid velocity of section 2-2 (m/s).

For viscous fluids, the Bernoulli equation can be expressed as $H_1 + \frac{P_1}{\rho g} + \frac{v_1^2}{2g} = H_2 + \frac{P_2}{\rho g} + \frac{v_2^2}{2g} + \Delta E_{12}$, where ΔE_{12} represents the energy loss during fluid flow [21,22]. The total length of the joint accounts for a small proportion of the length of the whole drill string, so the head loss caused by sudden contraction and expansion is mainly considered in the joint section. Therefore, according to Bernoulli's principle,

$$H_1 + \frac{P_1}{\rho g} + \frac{v_1^2}{2g} = H_2 + \frac{P_2}{\rho g} + \frac{v_2^2}{2g} + h_{s,12} \tag{2}$$

In the formula,

$$h_{s,12} = \frac{\Delta P_{s,12}}{\gamma} = \frac{\Delta P_{s,12}}{\rho g} \tag{3}$$

where H_1 is the height of section 1-1 (m), H_2 is the height of section 2-2 (m), P_1 is the drilling fluid pressure of section 1-1 (Pa), P_2 is the drilling fluid pressure of section 2-2 (Pa), $h_{s,12}$ is the head loss caused by sudden contraction (m), $\Delta P_{s,12}$ is the surge pressure in the sudden contraction section (Pa), g is the gravitational acceleration (m/s^2).

In the process of drilling fluid flowing from section 1-1 to section 2-2, the momentum conservation equation is

$$P_1 A_1 - P_{12}(A_1 - A_2) - P_2 A_2 = \rho Q_{v,2} v_2 - \rho Q_{v,1} v_1 \tag{4}$$

where P_{12} is the pressure on the annular area of the sudden contraction section (Pa), $Q_{v,1}$ is the volume flow rate of drilling fluid at section 1-1 (m^3/s), $Q_{v,2}$ is the volume flow rate of drilling fluid at section 2-2 (m^3/s).

The research shows that the pressure distribution on the annular area of the sudden shrinkage section is nearly consistent with the hydrostatic pressure distribution [23], that is, $P_{12} = P_1$, simplifying the above equation to

$$P_1 - P_2 = \rho v_2^2 - \rho v_2 v_1 \quad (5)$$

By combining Equations (1)–(3) and Equation (5), the surge pressure caused by the sudden contraction of the tool joint can be obtained.

$$\begin{cases} \Delta P_{s,12} = \rho g \left[(H_1 - H_2) + \frac{P_1 - P_2}{\rho g} + \frac{v_1^2 - v_2^2}{2g} \right] \\ P_2 = P_1 - \rho (v_2^2 - v_2 v_1), v_2 = \frac{A_1 v_1}{A_2} \end{cases} \quad (6)$$

For the horizontal pipeline ($H_1 = H_2$), Equation (6) can be simplified as,

$$\Delta P_{s,12} = \frac{\rho (v_1 - v_2)^2}{2} \quad (7)$$

Furthermore,

$$h_{s,12} = \frac{\Delta P_{s,12}}{\rho g} = \frac{(v_1 - v_2)^2}{2g} = \left(1 - \frac{A_2}{A_1}\right)^2 \frac{v_2^2}{2g} \quad (8)$$

The above equation is consistent with the head loss equation in the sudden retraction section given by Jeong and Shah [16].

2.1.2. The Sudden Expansion Pipe

Similarly, in the process of drilling fluid flowing from section 2-2 to section 3-3, according to the constant mass flow rate of drilling fluid.

$$\rho A_2 v_2 = \rho A_3 v_3 \quad (9)$$

where A_3 is the annular cross-sectional area of section 3-3 (m^2), v_3 is the annular drilling fluid velocity of section 3-3 (m/s).

According to Bernoulli's principle [21,22],

$$H_2 + \frac{P_2}{\rho g} + \frac{v_2^2}{2g} = H_3 + \frac{P_3}{\rho g} + \frac{v_3^2}{2g} + h_{s,23} \quad (10)$$

$$h_{s,23} = \frac{\Delta P_{s,23}}{\gamma} = \frac{\Delta P_{s,23}}{\rho g} \quad (11)$$

where H_3 is the height of the section 3-3 (m), P_3 is the drilling fluid pressure of the section 3-3 (Pa), $h_{s,23}$ is the head loss caused by sudden expansion (m), $\Delta P_{s,23}$ is the surge pressure in the sudden expansion section (Pa).

The following equation can be obtained based on the law of conservation of momentum.

$$P_2 A_2 + P_{23} (A_3 - A_2) - P_3 A_3 = \rho Q_{v,3} v_3 - \rho Q_{v,2} v_2 \quad (12)$$

where P_{23} is the pressure on the annular area of the sudden expansion section (Pa), $Q_{v,3}$ is the volume flow rate of drilling fluid at section 3-3 (m^3/s).

$P_{23} = P_2$, simplify Equation (12).

$$P_2 - P_3 = \rho v_3^2 - \rho v_3 v_2 \quad (13)$$

By combining Equations (9)–(11) and Equation (13), the surge pressure caused by the sudden expansion of the tool joint can be obtained.

$$\begin{cases} \Delta P_{s,23} = \rho g \left[(H_2 - H_3) + \frac{P_2 - P_3}{\rho g} + \frac{v_2^2 - v_3^2}{2g} \right] \\ P_3 = P_2 - \rho(v_3^2 - v_2^2), v_3 = \frac{A_2 v_2}{A_3} \end{cases} \quad (14)$$

For the horizontal pipeline ($H_1 = H_2$), Equation (14) can be simplified as:

$$\Delta P_{s,23} = \frac{\rho(v_2 - v_3)^2}{2} \quad (15)$$

Then,

$$h_{s,23} = \frac{\Delta P_{s,23}}{\rho g} = \frac{(v_2 - v_3)^2}{2g} = \left(1 - \frac{A_3}{A_2}\right)^2 \frac{v_2^2}{2g} \quad (16)$$

The above equation is consistent with the head loss equation in the sudden expansion section given by Jeong and Shah [16].

2.2. Annular Drilling Fluid Velocity

As shown in Figure 2, the drill string will displace the bottom drilling fluid into the annulus and the pipe while tripping. Therefore, the annular drilling fluid will generate an upward flow rate. Moreover, the research of Clark et al. [9,24] showed that when the drill string moves up and down, the drilling fluid will flow due to “clinging”. Therefore, the annular drilling fluid flow rate consists of two parts, namely, the drilling fluid flow rate caused by the displacement of the drill string and the drilling fluid flow rate caused by “clinging”. The equation is as follows. In the equation, K is the clinging constant related to the annulus geometry (ratio of the drill string’s outer diameter to the wellbore’s diameter). The value of K can be obtained by referring to the chart provided by Burkhardt [9].

$$V_a = v_p \left[\frac{1}{D_w^2 - D_{d,o}^2} \cdot \frac{(D_{d,o,B}^2 - D_{d,i,B}^2)(D_{w,B}^2 - D_{d,o,B}^2)}{D_{w,B}^2 - D_{d,o,B}^2 + D_{d,i,B}^2} + K \right] \quad (17)$$

where V_a is the annular drilling fluid velocity (m/s), v_p is the tripping speed (m/s), D_w is the wellbore diameter (m), $D_{d,o}$ is the drill string outer diameter (m), D_w is the wellbore diameter (m), $D_{w,B}$ is the bottom wellbore diameter (m), $D_{d,o,B}$ is the bottom drill string outer diameter (m), $D_{d,i,B}$ is the bottom drill string inner diameter (m), K is the clinging constant.

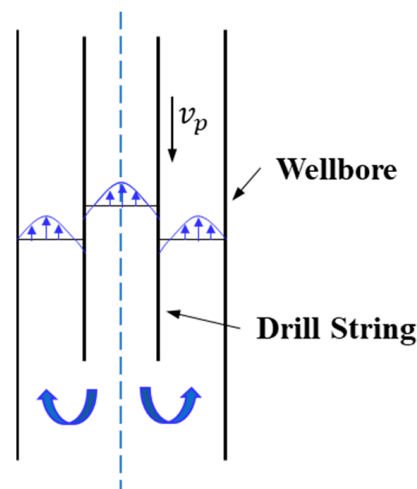


Figure 2. Drilling fluid flow state during the running of the open pipe.

3. Establishment of Wellbore Flow and Heat Transfer Model

3.1. Wellbore Flow Model

3.1.1. Governing Equations

- (1) Mass conservation equation

$$\frac{\partial(\rho_a v_a A_a)}{\partial x} = 0 \quad (18)$$

where ρ_a is the annular drilling fluid density (kg/m^3), v_a is the annular drilling fluid velocity (m/s), A_a is the annular cross-sectional area (m^2), x is the wellbore depth (m).

- (2) Momentum conservation equation

$$\frac{\partial(\rho_a v_a^2)}{\partial x} + \frac{\partial(P_a)}{\partial x} = -\rho_a g \cos \theta - P_s \quad (19)$$

where P_a is the annular drilling fluid pressure (Pa), P_s is the surge pressure (Pa/m), θ is the inclination angle ($^\circ$).

3.1.2. Model Solving

- (1) Grid division

As shown in Figure 3, if the wellbore is divided into n_x sections, there are N_x ($N_x = n_x + 1$) nodes (for storing parameters such as pressure, temperature, velocity, density, etc.). The wellhead and the bottom of the well are denoted as 1 and N_x , respectively.

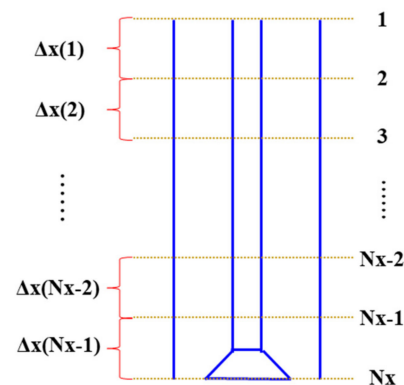


Figure 3. Schematic diagram of wellbore node division.

- (2) Discrete governing equations

Using the finite difference method to discretize the governing Equations (18) and (19).

$$\begin{cases} (Q_v)_i = \frac{(Q_m)_{i-1}}{(\rho)_i} \\ (P_a)_i = (P_a)_{i-1} - [(\rho_a v_a^2)_i - (\rho_a v_a^2)_{i-1}] + \\ (\Delta x)_{i-1} \frac{(\rho_a g \cos \theta)_{i-1} + (\rho_a g \cos \theta)_i}{2} + (\Delta x)_{i-1} \frac{(P_s)_{i-1} + (P_s)_i}{2} \end{cases} \quad (20)$$

where Q_m is the mass flow rate of drilling fluid (kg/s), Δx is the grid length (m).

- (3) Solving procedure

The iterative solution process of wellbore pressure is shown in Figure 4, which mainly includes the following steps: ① given the assumed value of node pressure; ② calculate the drilling fluid rheological parameters under different temperatures and pressures according to the assumed pressure value and wellbore temperature; ③ use the mass conservation equation to calculate the drilling fluid velocity; ④ calculate the nodal pressure based on the momentum conservation equation; ⑤ calculate the relative error between the assumed

pressure value and the calculated value to judge whether the assumed pressure value is reasonable; ⑥ if the relative error between the assumed pressure value and the calculated value is greater than the error bounds, update the assumed pressure value, and repeat steps ②–⑤ until the error is less than the error bounds; ⑦ if the relative error between the assumed pressure value and the calculated value is less than the error bounds, calculate the subsequent nodal pressure.

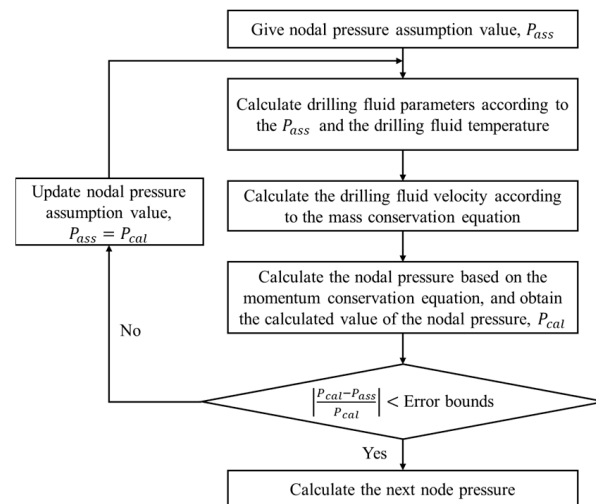


Figure 4. Wellbore pressure iterative solution process.

3.2. Wellbore Heat Transfer Model

Based on the energy conservation between formation and wellbore fluid, Kabir and Hasen et al. [25,26] established a differential governing equation of wellbore-formation heat transfer under the conditions of steady-state heat transfer in the wellbore and transient heat transfer in the formation and the analytical solution of wellbore fluid temperature calculation is given. The model established by Kabir et al., has high calculation accuracy and fast operation speed. This study is based on the model to calculate the drilling fluid temperature. It is coupled with wellbore pressure to determine the drilling fluid properties at different temperatures and pressures. The wellbore temperature calculation model is as follows:

$$\begin{cases} T_t = \alpha e^{\lambda_1 z} + \beta e^{\lambda_2 z} + g_G z - B g_G + T_{es} \\ T_a = (1 + \lambda_1 B) \alpha e^{\lambda_1 z} + (1 + \lambda_2 B) \beta e^{\lambda_2 z} + g_G z + T_{es} \end{cases} \quad (21)$$

$$\begin{cases} \alpha = -\frac{(T_{ti} + B g_G - T_{es}) \lambda_2 e^{\lambda_2 L} + g_G}{\lambda_1 e^{\lambda_1 L} - \lambda_2 e^{\lambda_2 L}} \\ \beta = \frac{(T_{ti} + B g_G - T_{es}) \lambda_1 e^{\lambda_1 L} + g_G}{\lambda_1 e^{\lambda_1 L} - \lambda_2 e^{\lambda_2 L}} \\ \lambda_1 = \frac{1}{2A} + \frac{1}{2A} \sqrt{1 + \frac{4A}{B}}, \lambda_2 = \frac{1}{2A} - \frac{1}{2A} \sqrt{1 + \frac{4A}{B}} \\ A = \frac{c_{fl} w}{2\pi} \frac{k_e + r_w U_a T_D}{r_w U_a k_e}, B = \frac{w c_{fl}}{2\pi r_t U_t}, t_D = \frac{k_e t}{c_e \rho_e r_w^2} \\ T_D = \ln[e^{-0.2 t_D} + (1.5 - 0.3719 e^{-t_D}) \sqrt{t_D}] \end{cases} \quad (22)$$

where T_a is the annular drilling fluid temperature ($^{\circ}\text{C}$), T_t is the tubing drilling fluid temperature ($^{\circ}\text{C}$), T_{ti} is the inlet drilling fluid temperature ($^{\circ}\text{C}$), T_{es} is the surface earth temperature ($^{\circ}\text{C}$), g_G is the geothermal gradient ($^{\circ}\text{C}/\text{m}$), c_{fl} is the drilling fluid specific heat capacity ($\text{J}/(\text{kg} \cdot ^{\circ}\text{C})$), c_e is the formation specific heat capacity ($\text{J}/(\text{kg} \cdot ^{\circ}\text{C})$), k_e is the earth thermal conductivity ($\text{W}/\text{m} \cdot ^{\circ}\text{C}$), U is the overall heat-transfer coefficient ($\text{W}/\text{m}^2 \cdot ^{\circ}\text{C}$), T_D is the dimensionless temperature, t_D is the dimensionless circulation time, t is the circulation time (h), w is the mass flow rate (kg/s), ρ_e is formation density (kg/m^3), L is the overall well depth (m), z is the well depth (m), r_w is the wellbore radius (m), r_t is the tubing radius (m).

3.3. Prediction Model of HTHP Fluid Properties

Under the condition of HTHP, the properties of drilling fluid are greatly affected by temperature and pressure [27,28]. Previous researchers have carried out a large number of studies on the properties of HTHP drilling fluids. Among them, the research on the prediction model of HTHP fluid properties mainly includes two categories: the empirical model and the compositional model. Because of the simple process of establishing the empirical model, the convenience of use and the high precision, it is more widely used. This study used the empirical model of HTHP drilling fluid properties proposed by Minton and Bern [29]. The model can better reflect the relationship between the properties of drilling fluid and temperature and pressure.

$$f(T, P) = f(T_0, P_0)e^{\alpha(T-T_0)+\beta(P-P_0)} \quad (23)$$

where $f(T, P)$ is the drilling fluid density or rheological parameters, T_0 is the drilling fluid test temperature ($^{\circ}\text{C}$), P_0 is the drilling fluid test pressure (Pa), T is the drilling fluid temperature ($^{\circ}\text{C}$), P is the drilling fluid pressure (Pa), α is the coefficient, β is the coefficient.

4. Model Validation

Clark and Fontenot [30] conducted a field test of swab/surge pressure for a well in Utah, and gave detailed test parameters and results. To verify the accuracy and applicability of the surge pressure prediction model, this paper uses the experimental data published by Clark to calculate the surge pressure and compare it with the measured data. The parameter settings and test results of the field experiments involved in this section are all field experiments carried out by Clark and Fontenot.

The depth of the experimental well was 4654 m, and the depth of the drill string was 4591 m. The drill string was mainly composed of four parts: drill pipe, drill collar, joint, and carrier (carrier was used to test the downhole temperature and pressure of drilling fluid). The schematic diagram of the wellbore-drill string structure is shown in Figure 5. The joint parameters are not given. After consulting the API drill pipe-joint specification, it is known that the common joint outer diameters of the drill pipes with outer diameters of 73 and 88.9 mm were 105 and 127 mm, respectively. In the calculation process, the length of each drill pipe or drill collar was taken as 9.144 m, and the length of a single joint was taken as 0.50 m. The carrier consisted of three sections, the length was relatively short and the outer diameter was significantly larger than the outer diameter of the drill string, which could be treated as a joint.

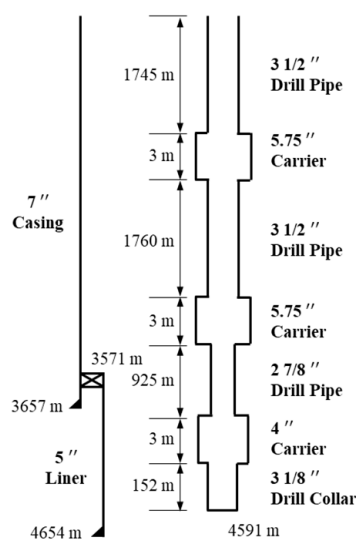


Figure 5. Wellbore-drill string geometries in Utah well.

In the field test, a water-based drilling fluid with a density of 1701.54 kg/m³ was used. During the experiment, drilling fluid samples were collected every 15 min, and parameters such as density, yield point, and plastic viscosity were tested. The results of each measurement are shown in Table 1. The average density of the drilling fluid was 1693.59 kg/m³ (this value is used as the density of drilling fluid calculated by surge pressure in this section), and the measured values of yield point and plastic viscosity were pretty different.

Table 1. Room temperature properties of drilling fluid during test.

Time Collected	Density (kg/m ³)	YP (Pa)	PV (mPa · s)
6:00	1689.18	0.00	24.00
6:15	1689.18	0.00	24.00
6:30	1689.18	0.00	31.00
6:45	1713.14	0.96	37.00
7:00	1701.16	1.92	43.00
7:15	1713.14	9.58	39.00
7:30	1713.14	8.62	42.00
7:45	1713.14	3.35	43.00
8:00	1725.12	1.44	40.00
8:15	1677.20	1.92	35.00
8:30	1677.20	0.48	34.00
8:45	1677.20	0.00	28.00
9:00	1689.18	0.00	32.00
9:15	1677.20	0.00	35.00
9:30	1689.18	0.00	41.00
9:45	1689.18	0.48	37.00
10:00	1665.22	1.92	34.00
10:15	1701.16	12.93	50.00
10:30	1689.18	4.79	39.00

In addition, Clark and Fontenot also tested the yield point and plastic viscosity of drilling fluids in the range of 30–120 °C and they plotted the above parameters as a function of temperature. Based on this curve, the rheological parameters of drilling fluid at different temperatures were extracted. The data are shown in Table 2.

Table 2. Results of yield point and plastic viscosity of drilling fluid at different temperatures.

Serial Number	Temperature (°C)	YP (Pa)	PV (mPa · s)
1	30	0.14	30.20
2	38	0.19	25.10
3	45	0.29	21.90
4	52	0.43	18.30
5	59	0.62	17.00
6	66	0.86	16.50
7	73	1.15	15.20
8	80	1.72	14.70
9	86	2.35	14.30
10	93	3.11	13.90
11	100	4.02	14.00
12	107	5.12	14.50
13	114	6.66	15.90
14	120	8.05	16.60

Taking the natural logarithm of both sides of Equation (23).

$$\ln f(T, P) = \ln f(T_0, P_0) + \alpha(T - T_0) + \beta(P - P_0) \quad (24)$$

Simplify the above equation.

$$\ln \frac{f(T, P)}{f(T_0, P_0)} = \alpha(T - T_0) + \beta(P - P_0) \quad (25)$$

$$\text{Let } y = \ln \frac{f(T, P)}{f(T_0, P_0)}, x_1 = T - T_0, x_2 = P - P_0.$$

$$y = \alpha x_1 + \beta x_2 \quad (26)$$

Based on the test results of drilling fluid parameters at different temperatures and pressures, the prediction equation of HTHP drilling fluid parameters could be obtained by combining Equation (26) with the multiple linear regression method. Clark did not consider the influence of pressure on the properties of drilling fluid, and Equation (26) can be further simplified as:

$$y = \alpha x_1 \quad (27)$$

Take $T_0 = 30 \text{ }^\circ\text{C}$, $\tau_{y,0} = 0.14 \text{ Pa}$. The yield point prediction model was obtained by regression of the data in Table 2. The average relative error between the predicted value of the yield point and the actual value of the model was 8.86%, and the applicable temperature range was 30–120 $^\circ\text{C}$. The results are shown in Figure 6.

$$\tau_y(T) = \tau_{y,0} e^{0.0471(T-T_0)} \quad (28)$$

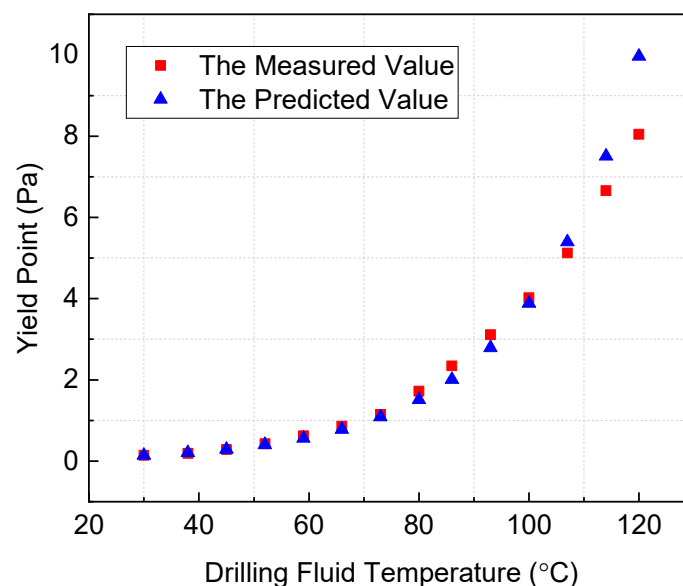


Figure 6. Comparison of predicted and measured yield point of drilling fluids.

The plastic viscosity of the drilling fluid measured by Clark does not change monotonically with temperature, and the model established by Equation (27) is ineffective. After comparing linear, exponential, logarithmic, polynomial and other models, it was found that the prediction accuracy of the polynomial model was higher, and the modeling was simple and easy to use. The drilling fluid plastic viscosity prediction model is as follows. The applicable temperature range is 30–120 $^\circ\text{C}$, and the average prediction accuracy is 97.02%. The results are shown in Figure 7.

$$\mu_p(T) = 0.0042T^2 - 0.7581T + 47.994 \quad (29)$$

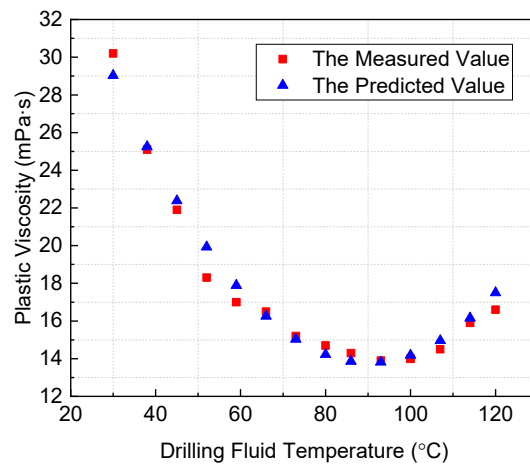


Figure 7. Comparison of predicted and measured plastic viscosity of drilling fluids.

Based on the above experimental parameters, Clark and Fontenot conducted wellbore swab/surge pressure testing experiments under different conditions. One set of the drill string tripping speed and surge pressure measurement results at a well depth of 4591 m is shown in Figures 8 and 9. The input speed was 0.7584 m/s, and the maximum value of the surge pressure was 9.3579 MPa.

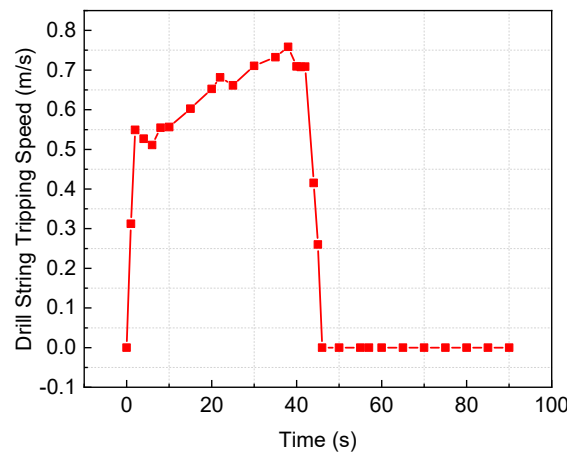


Figure 8. Drill string tripping speed vs. time.

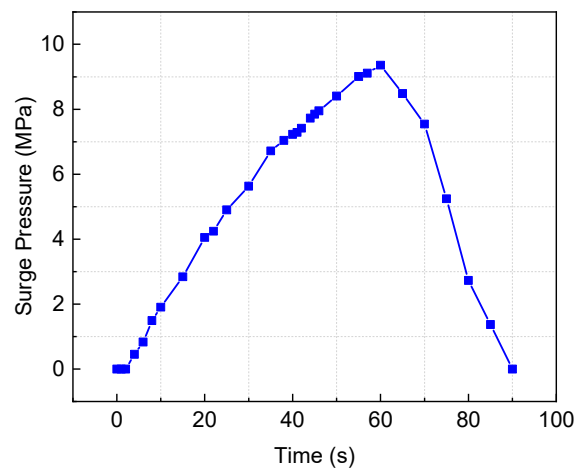


Figure 9. Surge pressure vs. time.

Calculations and analyses were performed using measured data from Clark and Fontenot. The surge pressure calculations under four conditions were carried out, namely: ① considering the effect of temperature and pressure on the fluid, considering the effect of the joint (Case 1); ② considering the effect of temperature and pressure on the fluid, ignoring the effect of the joint (Case 2); ③ ignoring the effect of temperature and pressure on the fluid, considering the effect of the joint (Case 3); ④ the influence of temperature and pressure on the fluid and the influence of joints not being considered (Case 4).

Although Clark and Fontenot measured the plastic viscosity and yield point of the drilling fluid several times during the experiment (i.e., Table 1), the measured values of plastic viscosity and yield point were quite different. Therefore, in this study, the average value of plastic viscosity and the yield point of the drilling fluid when temperature and pressure were considered to calculate the surge pressure when temperature and pressure were not considered.

Clark and Fontenot did not provide parameters related to the wellbore temperature field, but calculating the wellbore temperature field requires parameters such as geothermal gradient and formation thermal conductivity. Therefore, based on the literature research and previous work experience, the main parameters needed for calculating the wellbore temperature field were determined. The main parameters are shown in Table 3.

Table 3. Main parameter settings for wellbore temperature calculation.

Parameter	Value
Surface earth temperature (°C)	20
Inlet drilling fluid temperature (°C)	20
Formation density (kg/m ³)	2650
Geothermal gradient (°C/100 m)	2.4
Earth thermal conductivity (W/(m · °C))	2.25
Drilling fluid specific heat capacity (J/(kg · °C))	1600
Formation specific heat capacity (J/(kg · °C))	800
Circulation time (h)	10

First, without considering the effects of temperature and joints, the bottom hole ECD at different drill string tripping speeds was compared with WellPlan, and the results are shown in Figure 10. The drilling fluid density was 1693.59 kg/m³. It can be seen that the ECD of the bottom hole will increase when the drill string is run, and it increases with the increase in the speed of the drill string. According to the analysis, the main reason is that the higher the drilling speed of the drill string, the higher the surge pressure, and the more the increase in the bottom hole ECD. In addition, the average relative error between the model calculation results and WellPlan calculation results was 0.0258%, and the reliability of the calculation results was high.

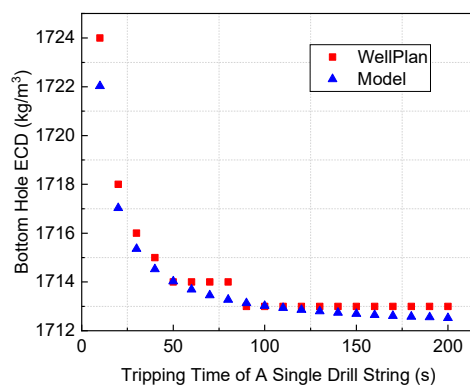


Figure 10. Bottom hole ECD comparison regardless of temperature and joint effects.

The calculation results of wellbore surge pressure under four different conditions are shown in Figure 11. The annulus drilling fluid temperature and rheological parameters are shown in Figures 12 and 13. The maximum tripping speed of the drill string was 0.7584 m/s, and the maximum measured value of the surge pressure was 9.3579 MPa. The maximum values of the calculated value of the surge pressure in the four cases were 9.2757, 1.3440, 10.5171, and 1.2205 MPa. Among them, the calculated value of the surge pressure in Case 3 was the largest, and the calculated value in Case 4 was the smallest. The difference between the two was more than 8 times. This result shows that the existence of joints will increase the surge pressure, but it does not mean that the existence of joints significantly affects the increase in wellbore surge pressure. The main reason is that the gap between the joint's outer diameter and the wellbore's diameter in this example was small, significantly influencing the surge pressure. However, if the annular gap between the joint and the wellbore is large, the impact on the surge pressure is not necessarily significant. Compared with the true value, the results considering the joint effect (Case 1 and Case 3) were significantly better than those without the joint effect (Case 2 and Case 4). Moreover, considering both the effect of temperature and pressure on the fluid and the influence of the joint (Case 1), the calculated value of the surge pressure was in the best agreement with the real value, and the relative error was only 0.89%.

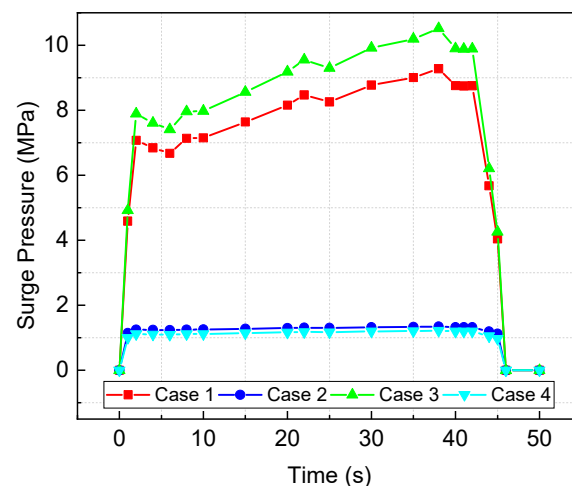


Figure 11. Comparison of predicted and measured values of surge pressure under different conditions.

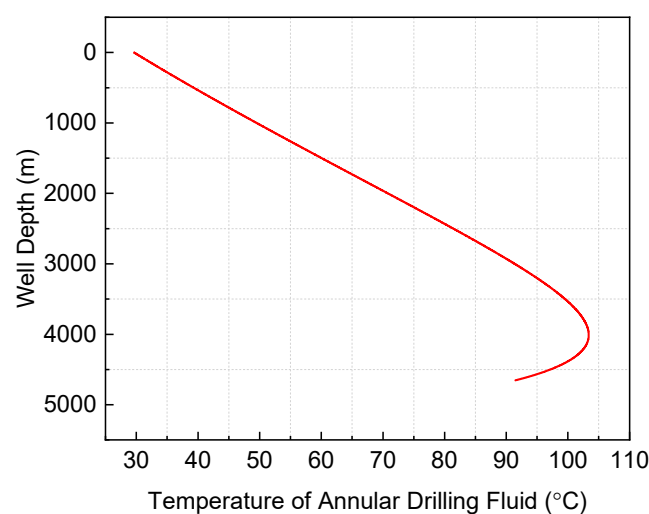


Figure 12. Variation curve of annular drilling fluid temperature with well depth.

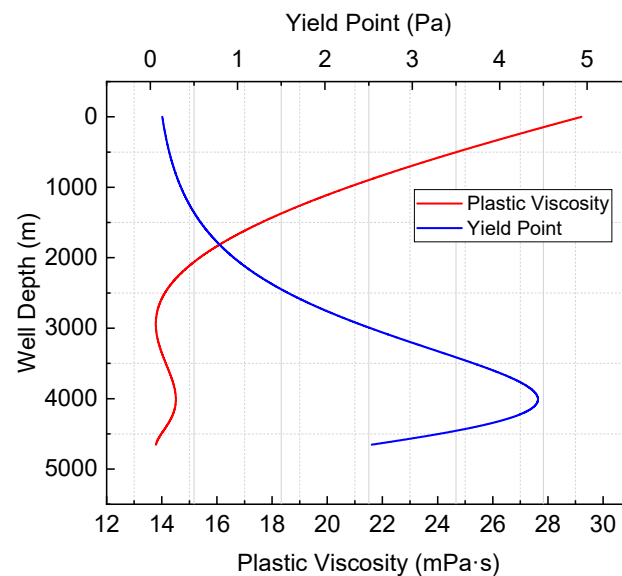


Figure 13. Variation curve of drilling fluid plastic viscosity and yield point with well depth.

5. Results and Discussions

In order to study the influence of dimensionless joint outer diameter (the ratio of joint outer diameter to wellbore diameter), joint length and drill string tripping speed on surge pressure, in this paper, the calculation and analysis of surge pressure were carried out based on the actual data of a well. The main parameters of the example were set as shown in Table 4.

Table 4. Parameter setting of surge pressure calculation.

Parameter		Value
Total well depth (m)		5700
Casing inner diameter (mm)	0–5700 m	215.9
Drill pipe diameter (mm)	0–2330 m	Inner: 107.7 Outer: 127.0
	2330–5700 m	Inner: 129.9 Outer: 149.2
Drilling fluid	Density (kg/m^3)	1600
	YP (Pa)	10
	PV ($\text{mPa} \cdot \text{s}$)	60
	Test temperature ($^{\circ}\text{C}$)	20
	Test pressure (MPa)	0.1
A single drill string	Length (m)	9.144
	Tripping time (s)	5, 10, 20, 30, 40, 50, 60, 70, 80, 90, 100, 110, 120, 130, 140, 150, 160, 170, 180, 190, 200
Tool joint	Outer diameter (mm)	152, 160, 172, 184, 197
	dimensionless tool joint outer diameter	0.704, 0.741, 0.797, 0.852, 0.912
	Overall length (m)	0, 50, 100, 150, 200, 250, 300
Pump rate (m^3/min)		0.1, 0.2, 0.3, 0.4, 0.5

5.1. The Influence of Dimensionless Joint Outer Diameter

The dimensionless joint outer diameters in the calculation example were 0.704, 0.741, 0.797, 0.852, and 0.912, respectively. The relationship between the bottom hole ECD and the dimensionless joint outer diameter is shown in Figure 14. The relationship between the surge pressure and the dimensionless joint outer diameter is shown in Figure 15. It was found that the bottom hole ECD and surge pressure increase with the increase in the

dimensionless joint outer diameter. The main reason is that the smaller the annular gap, the higher the annular drilling fluid flow rate and the higher the surge pressure caused by the drill string tripping. Moreover, the clinging constant of drilling fluid under a narrow annular gap is higher, and the clinging effect of annular fluid is more significant, which will also cause an increase in surge pressure.

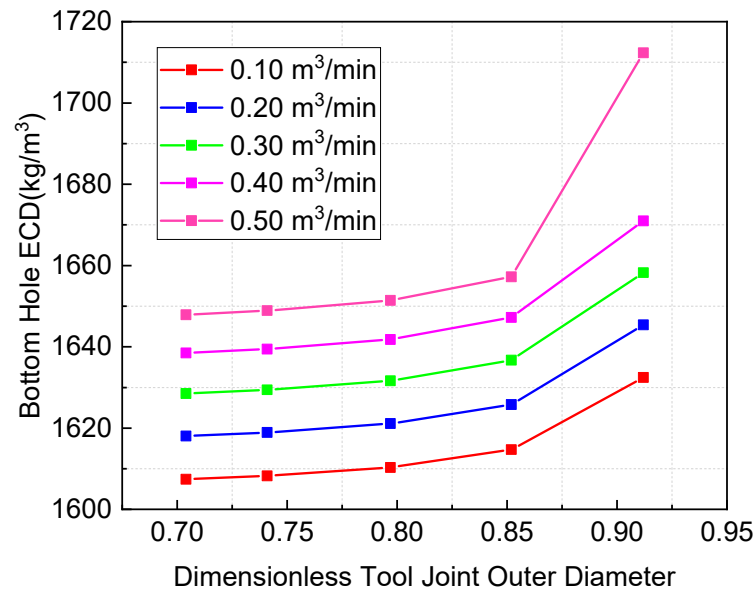


Figure 14. The relationship between the bottom hole ECD and the dimensionless tool joint outer diameter.

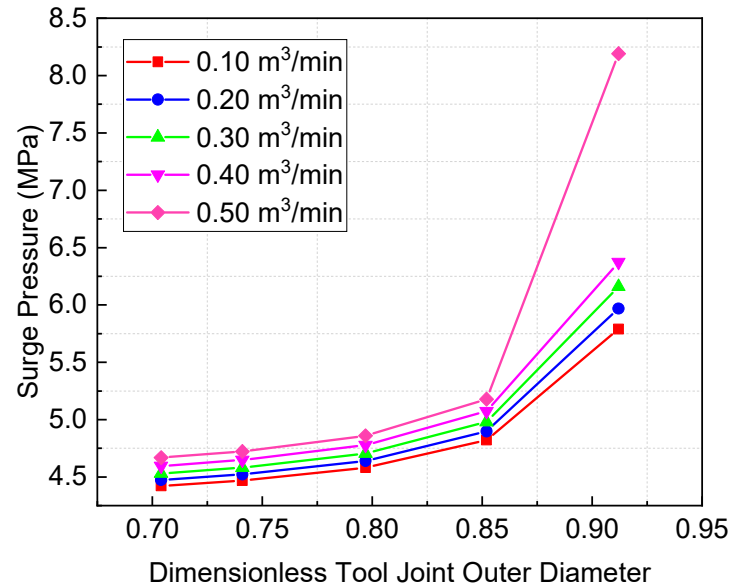


Figure 15. The relationship between the surge pressure and the dimensionless tool joint outer diameter.

Figure 16 describes the relationship between the surge pressure difference and the dimensionless joint outer diameter (surge pressure difference = surge pressure when the joint exists—surge pressure when the joint does not exist). It can be seen from Figure 16 that the values of the surge pressure difference were all positive values, indicating that the existence of the joint increases the surge pressure. Moreover, the surge pressure was increased by a maximum of 76% compared to the surge pressure that did not consider the joint's existence.

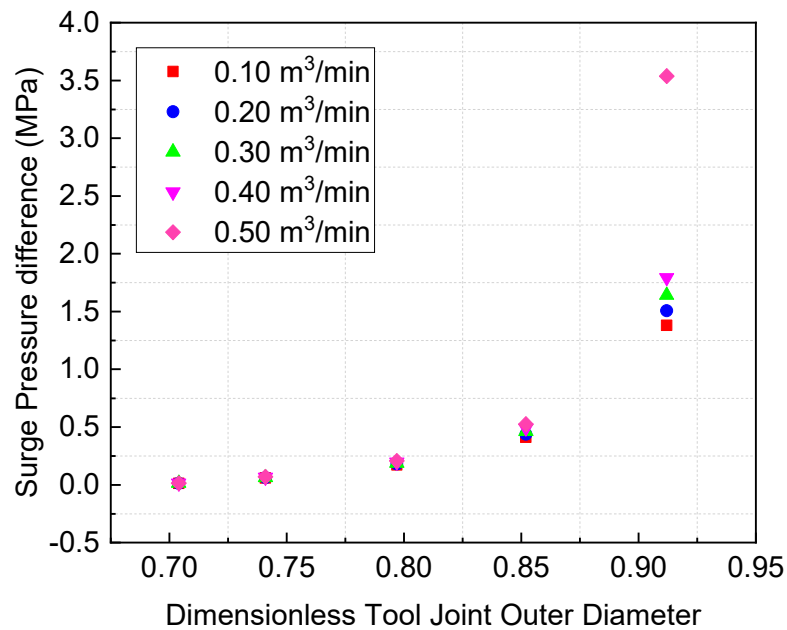


Figure 16. The difference between the surge pressure when the tool joint is considered and the surge pressure when the joint is not considered.

5.2. The Influence of Joint Length

Figures 17 and 18 show the effect of overall joint length on bottom hole ECD and surge pressure. The overall length of the joint was set to 0, 50, 100, 150, 200, 250, and 300 m, where the overall joint length of 0 m represents the situation without considering the existence of the joint. The analysis results showed that the longer the overall length of the joint, the greater the bottom hole ECD and surge pressure. With the increase in the dimensionless joint outer diameter, the the bottom hole ECD and the surge pressure also increased. Furthermore, it can be observed that the surge pressure increased almost linearly with the length of the joint.

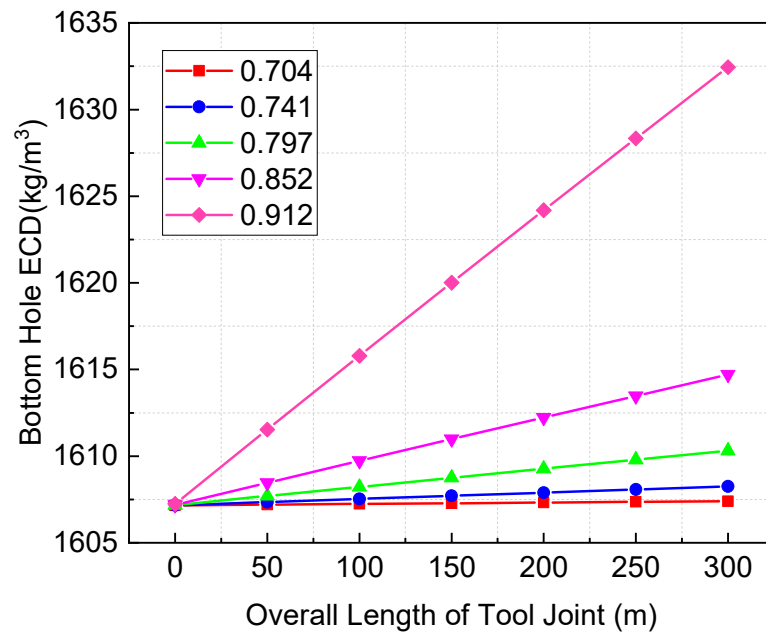


Figure 17. Bottom hole ECD vs. overall length of tool joint.

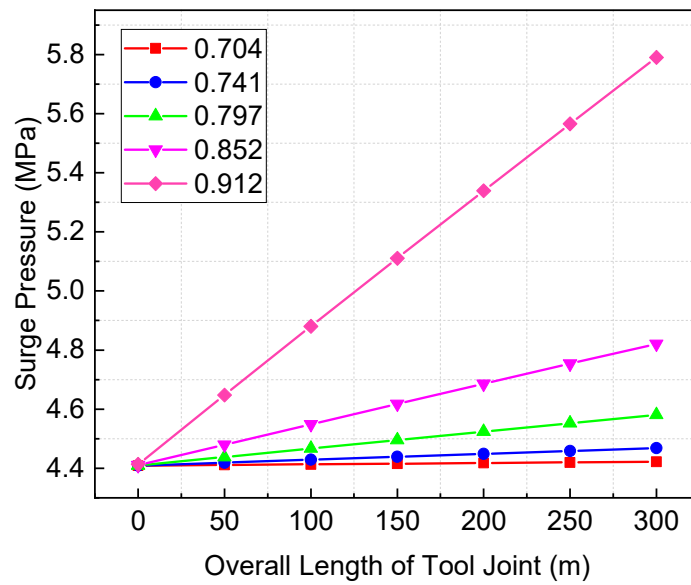


Figure 18. Surge pressure vs. overall length of tool joint.

5.3. The Influence of Drill String Tripping Speed

Adjusting the tripping speed of the drill string is a convenient and effective method to control the surge pressure of the wellbore during tripping. This study’s tripping speed determination was mainly based on the parameter settings of previous field experiments. Among them, the maximum tripping speed of Burkhardt’s experiments was about 6 ft/s = 1.8288 m/s [9]. In the calculation example, the length of a single drill string was 9.144 m, and the tripping time of a single drill string was set to 5, 10, 20 . . . 200 s. Therefore, the tripping speed was 0.0457–1.8288 m/s. The calculation example shows that the bottom hole ECD and surge pressure increased with the drill string tripping speed. The faster the drill string ran, the higher the bottom hole ECD and surge pressure increased. When the drill string tripping speed gradually decreased and tended to a stable value, the bottom hole ECD also tended to a stable value. The results are shown in Figures 19 and 20.

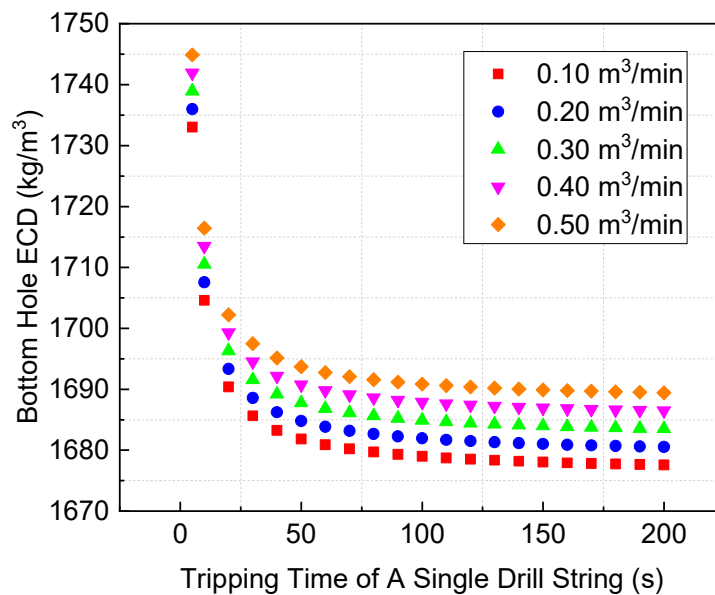


Figure 19. Variation of bottom hole ECD with tripping time of a single drill string.

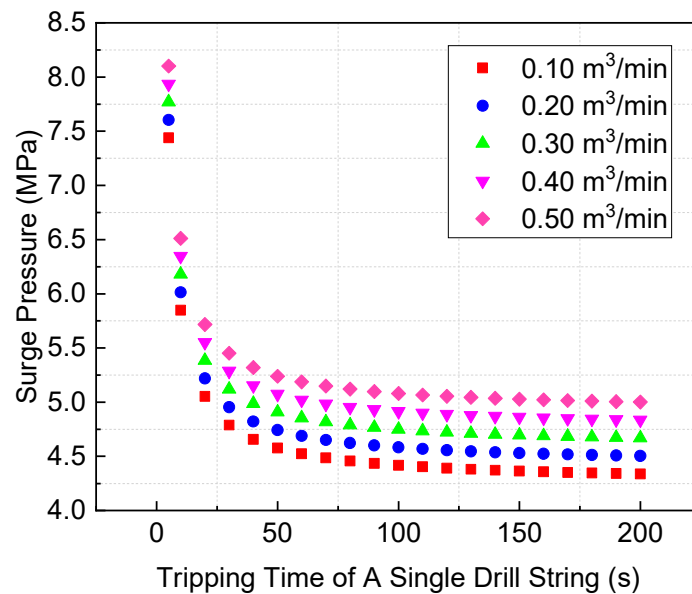


Figure 20. Variation of surge pressure with tripping time of a single drill string.

6. Conclusions

In this paper, the research into surge pressure was carried out, and the following main points were obtained.

- Based on the fundamental laws of fluid mechanics, the calculation equation of the surge pressure at the joint was deduced. A calculation model of surge pressure in HTHP wells was established considering the influence of joints.
- The surge pressure prediction results were compared with the measured data. The relative error was only 0.89%. The accuracy of the surge pressure prediction model is high.
- The influence of joint and tripping speed on surge pressure was analyzed. The existence of joints increases the surge pressure. The joint can significantly affect the surge pressure when the annular gap is small. The faster the drill string is tripped, the greater the surge pressure.
- During the drilling operation, the safe tripping operation can be ensured by reducing the outer joint diameter and the tripping speed.

Author Contributions: Conceptualization, J.S. and X.S.; methodology, B.Y.; validation, J.S. and Y.G.; formal analysis, X.S.; investigation, J.S., X.S. and B.Y.; resources, Y.G.; writing—original draft preparation, J.S. and B.Y.; writing—review and editing, X.S. and Y.G. All authors have read and agreed to the published version of the manuscript.

Funding: This research received no external funding.

Acknowledgments: The authors express their sincere thanks to the authors of the references in the manuscript.

Conflicts of Interest: The authors declare no conflict of interest.

References

1. Bourgoyne, A.T.; Millheim, K.K.; Chenevert, M.E.; Young, F.S. *Applied Drilling Engineering*; Society of Petroleum Engineers: Richardson, TX, USA, 1986; Volume 2.
2. Mohammad, A.; Davidrajuh, R. Modeling of Swab and Surge Pressures: A Survey. *Appl. Sci.* **2022**, *12*, 3526. [[CrossRef](#)]
3. Al-Abduljabbar, A.; Hossain, M.E.; Gharbi, S.A.; Al-Rubaii, M. Optimization of tripping speed to minimize surge & swab pressure. In Proceedings of the SPE/IADC Middle East Drilling Technology Conference and Exhibition, Abu Dhabi, United Arab Emirates, 29–31 January 2018. [[CrossRef](#)]
4. Feng, G.; Xie, Z. Research on drilling engineering technology under high temperature and pressure at extra deep exploration well in Fergana basin and its application. *Xinjiang Oil Gas* **2011**, *7*, 21–27.

5. Shaughnessy, J.M.; Romo, L.A.; Soza, R.L. Problems of ultra-deep high-temperature, high-pressure drilling. In Proceedings of the SPE Annual Technical Conference and Exhibition, Denver, CO, USA, 5–8 October 2003. [[CrossRef](#)]
6. Cannon, G.E. Changes in Hydrostatic Pressure Due to Withdrawing Drill Pipe from the Hole. In *Drilling and Production Practice*; OnePetro: Richardson, TX, USA, 1934.
7. Goins, W.; Weichert, J.; Burba, J.; Dawson, D.; Teplitz, A. Down-the-hole pressure surges and their effect on loss of circulation. In *Drilling and Production Practice*; OnePetro: Richardson, TX, USA, 1951.
8. Cardwell, W. Pressure changes in drilling wells caused by pipe movement. In *Drilling and Production Practice*; OnePetro: Richardson, TX, USA, 1953.
9. Burkhardt, J. Wellbore pressure surges produced by pipe movement. *J. Pet. Technol.* **1961**, *13*, 595–605. [[CrossRef](#)]
10. Schuh, F. Computer makes surge-pressure calculations useful. *Oil Gas J.* **1964**, *31*, 96.
11. Fontenot, J.E.; Clark, R. An improved method for calculating swab and surge pressures and circulating pressures in a drilling well. *Soc. Pet. Eng. J.* **1974**, *14*, 451–462. [[CrossRef](#)]
12. Lubinski, A.; Hsu, F.; Nolte, K. Transient pressure surges due to pipe movement in an oil well. *Rev. L'institut Français Pétrole* **1977**, *32*, 307–348. [[CrossRef](#)]
13. Lal, M. Surge and swab modeling for dynamic pressures and safe trip velocities. In Proceedings of the IADC/SPE Drilling Conference, New Orleans, LA, USA, 20–23 February 1983. [[CrossRef](#)]
14. Mitchell, R. Dynamic surge/swab pressure predictions. *SPE Drill. Eng.* **1988**, *3*, 325–333. [[CrossRef](#)]
15. Zhong, B.; Zhou, K.; Xie, Q. Theoretical study on steady-state surge pressure in eccentric annulus. *J. Southwest Pet. Univ.* **1995**, *17*, 38.
16. Jeong, Y.-T.; Shah, S.N. Analysis of tool joint effects for accurate friction pressure loss calculations. In Proceedings of the IADC/SPE Drilling Conference, Dallas, TX, USA, 2–4 March 2004. [[CrossRef](#)]
17. Srivastav, R.; Enfis, M.; Crespo, F.; Ahmed, R.; Saasen, A.; Laget, M. Surge and swab pressures in horizontal and inclined wells. In Proceedings of the SPE Latin America and Caribbean Petroleum Engineering Conference, Mexico City, Mexico, 16–18 April 2012. [[CrossRef](#)]
18. Li, J.; Huang, Z.; Li, K.; Wu, W. The influence of collar on surge pressure caused by the drilling fluid viscous force under pumping condition. *Res. J. Appl. Sci. Eng. Technol.* **2013**, *5*, 1781–1785. [[CrossRef](#)]
19. Li, Q.; Wang, Z.; Li, X.; Shen, L. The computational model for surge pressure of Herschel-Bulkley fluid in eccentric annulus. *Acta Petroli Sinica* **2016**, *37*, 1187–1192.
20. Simoes, S.Q.; Miska, S.Z.; Takach, N.E.; Yu, M. The effect of tool joints on ECD while drilling. In Proceedings of the Production and Operations Symposium, Oklahoma City, OK, USA, 31 March–3 April 2007. [[CrossRef](#)]
21. Badeer, H.S.; Synolakis, C.E. The Bernoulli-Poiseuille equation. *Phys. Teach.* **1989**, *27*, 598–601. [[CrossRef](#)]
22. Synolakis, C.E.; Badeer, H.S. On combining the Bernoulli and Poiseuille equation—A plea to authors of college physics texts. *Am. J. Phys.* **1989**, *57*, 1013–1019. [[CrossRef](#)]
23. Fan, H. *Practical Drilling Fluid Mechanics*; Petroleum Industry Press: Beijing, China, 2014.
24. Clark, E. Bottom-hole pressure surges while running pipe. *Pet. Eng. Int.* **1955**, *27*, B68.
25. Hasan, A.; Kabir, C. Wellbore heat-transfer modeling and applications. *J. Pet. Sci. Eng.* **2012**, *86*, 127–136. [[CrossRef](#)]
26. Kabir, C.; Hasan, A.; Kouba, G.; Ameen, M. Determining circulating fluid temperature in drilling, workover, and well control operations. *SPE Drill. Complet.* **1996**, *11*, 74–79. [[CrossRef](#)]
27. Osisanya, S.O.; Harris, O.O. Evaluation of equivalent circulating density of drilling fluids under high pressure/high temperature conditions. In Proceedings of the SPE Annual Technical Conference and Exhibition, Dallas, TX, USA, 9–12 October 2005.
28. Polite, M. Invert oil mud rheology as a function of temperature and pressure. In Proceedings of the SPE/IADC Drilling Conference, New Orleans, LA, USA, 28 February–2 March 1985.
29. Minton, R.; Bern, P. Field measurement and analysis of circulating system pressure drops with low-toxicity oil-based drilling fluids. In Proceedings of the IADC/SPE Drilling Conference, Dallas, TX, USA, 28 February–2 March 1988. [[CrossRef](#)]
30. Clark, R.; Fontenot, J. Field measurements of the effects of drillstring velocity, pump speed, and lost circulation material on downhole pressures. In Proceedings of the Fall Meeting of the Society of Petroleum Engineers of AIME, Houston, TX, USA, 6–9 October 1974. [[CrossRef](#)]